frontiers in Catalysis

ORIGINAL RESEARCH
published: 21 January 2022
doi: 10.3389/fctls.2021.780474

Maximizing Photosynthesis-Driven Baeyer–Villiger Oxidation Efficiency in Recombinant *Synechocystis* sp. PCC6803

Adrian Tüllinghoff, Magdalena B. Uhl, Friederike E. H. Nintzel, Andreas Schmid, Bruno Bühler and Jörg Toepel**

Department Solar Materials, Helmholtz Centre for Environmental Research, Helmholtz Association of German Research Centres (HZ), Leipzig, Germany

OPEN ACCESS

Edited by:
Florian Rudroff, Vienna University of Technology, Austria

Reviewed by:
Shuke Wu, Huazhong Agricultural University, China
Oliver Spadiut, Vienna University of Technology, Austria

***Correspondence:**
Bruno Bühler
bruno.bühler@ufz.de
Jörg Toepel
joerg.toepel@ufz.de

Specialty section:
This article was submitted to Biocatalysis, a section of the journal Frontiers in Catalysis

Received: *21 September 2021*
Accepted: *14 December 2021*
Published: *21 January 2022*

Citation:
Tüllinghoff A, Uhl MB, Nintzel FEH, Schmid A, Bühler B and Toepel J (2022) Maximizing Photosynthesis-Driven Baeyer–Villiger Oxidation Efficiency in Recombinant Synechocystis sp. PCC6803. Front. Catal. 1:780474. doi: 10.3389/fctls.2021.780474

Photosynthesis-driven whole-cell biocatalysis has great potential to contribute to a sustainable bio-economy since phototrophic cells use light as the only energy source. It has yet to be shown that phototrophic microorganisms, such as cyanobacteria, can combine the supply of high heterologous enzyme levels with allocation of sufficient reduction equivalents to enable efficient light-driven redox biocatalysis. Here, we demonstrated that the heterologous expression of an NADPH-dependent Baeyer–Villiger monooxygenase (BVMO) gene from *Acidovorax* sp. CHX100 turns *Synechocystis* sp. PCC6803 into an efficient oxyfunctionalization biocatalyst, deriving electrons and O_2 from photosynthetic water oxidation. Several expression systems were systematically tested, and a *P*nrsB-(Ni^{2+})–controlled expression based on a replicative plasmid yielded the highest intracellular enzyme concentration and activities of up to 60.9 ± 1.0 U g_{CDW}^{-1}. Detailed analysis of reaction parameters, side reactions, and biocatalyst durability revealed—on the one hand—a high *in vivo* BVMO activity in the range of 6 ± 2 U mg_{BVMO}^{-1} and—on the other hand—an impairment of biocatalyst performance by product toxicity and by-product inhibition. Scale-up of the reaction to 2-L fed-batch photo-bioreactors resulted in the stabilization of the bioconversion over several hours with a maximal specific activity of 30.0 ± 0.3 U g_{CDW}^{-1}, a maximal volumetric productivity of 0.21 ± 0.1 gL^{-1} h^{-1}, and the formation of 1.3 ± 0.1 gL^{-1} of ε-caprolactone. Process simulations based on determined kinetic data revealed that photosynthesis-driven cyclohexanone oxidation on a 2-L scale under high-light conditions was kinetically controlled and not subject to a limitation by photosynthesis.

Keywords: whole-cell biocatalysis, photo-biotechnology, heterologous expression, scale-up, cyanobacteria, Baeyer–Villiger monooxygenase

INTRODUCTION

Biotechnological processes have been developed in the past decades to produce materials, chemicals, and pharmaceuticals (Schmid et al., 2001). Compared to standard chemical processes, they, in general, require less energy due to milder reaction conditions, produce less toxic byproducts, and use less harmful reagents, giving them high potential to be environmentally friendly (Burk and Van Dien, 2016); (Bornscheuer et al., 2012). While there are numerous feasible processes using enzymes as

catalysts or microbes as whole-cell factories, redox biocatalysis remains challenging (Schrewe et al., 2013). This is due to the dependence of redox enzymes on co-substrates such as electron carriers and O_2 (Law et al., 2006). When using isolated enzymes as catalysts, process efficiencies suffer high enzyme and cofactor regeneration costs (Kadisch et al., 2017). Applying whole cells bears the advantage to employ their metabolism to balance redox demands, for example, by oxidizing readily available organic compounds to enable electron supply. However, respective costs and high O_2 demands still often hinder efficient, stable, and cheap redox biocatalysis in heterotrophic cell factories (Baldwin and Woodley, 2006; Kadisch et al., 2017).

To overcome these issues, phototrophic microorganisms, such as the model cyanobacterium *Synechocystis* sp. PCC6803 (*Syn*6803 from here), are highly attractive host organisms for oxygenases (Lassen et al., 2014a; Lassen et al., 2014b; Böhmer et al., 2017; Hoschek et al., 2019b), reductases (Assil-Companioni et al., 2020), and hydrogenases (Appel et al., 2020). Their photosynthetic apparatus can be exploited to supply oxygenase reactions not only with reduction equivalents but also with O_2 from water and sunlight, the most environmentally friendly co-substrates (Hoschek et al., 2017). As whole-cell biocatalysts, cyanobacteria combine this advantage with their self-(re) generation capacity, relying on light, water, and CO_2 as main resources (Jodlbauer et al., 2021). Yet, phototrophs so far have gathered little attention as biocatalysts for regio-, chemo-, or stereoselective oxyfunctionalizations. Efforts to engineer cyanobacteria such as introducing a cytochrome P450 monooxygenase (CYP) (Berepiki et al., 2016), fusing a cytochrome P450 to a subunit of photosystem I (PS I) (Lassen et al., 2014a), or implementing CYP-dependent pathways (Wlodarczyk et al., 2015) remained on a proof-of-concept level.

Photosynthesis-driven oxyfunctionalization processes are hampered by a gap of knowledge regarding 1) sufficient gene expression (Lassen et al., 2014a), 2) protein stability and folding, and 3) cofactor supply. However, these aspects are of special importance to ensure that biocatalysis can be conducted in an efficient, stable, and host-compatible manner. Another hindrance for efficient photo-biotechnology are the high doubling times of cyanobacteria (8–12 h for *Syn*6803 (Heidorn et al., 2011)) and their light dependency, which limits high-density cultivation and scalability (Hoschek et al., 2019a).

High-level expression of heterologous genes in phototrophic organisms suffers a poorly developed molecular biology tool box compared to typical heterotrophic hosts (Berla et al., 2013). Specific characteristics such as the structure of the RNA polymerase (Imamura and Asayama, 2009), promoter types (Huang et al., 2010), and a circadian program (Johnson and Golden, 1999) are fundamental differences to well-studied heterotrophic hosts and often hamper transcriptional engineering (Camsund and Lindblad, 2014; Thiel et al., 2019). There are however pivotal recent developments such as the design of shuttle vectors (Huang et al., 2010) and expression studies focusing on promoters (Englund et al., 2016; Behle et al., 2020) and RBSs (Englund et al., 2016), utilized to increase product titers (Sebesta and Peebles, 2020). For detailed perspectives on regulatory systems and promoter types in cyanobacteria, the reader is referred to Gordon and Pfleger (2018); Immethun and Moon (2018); Gale et al. (2019); Till et al. (2020).

Recent studies employing oxygenases in *Syn*6803 already showed the accessibility of O_2 and electrons derived from the light reaction (Hoschek et al., 2019b). The employment of strictly NADPH-dependent oxygenases, such as cyclohexanone monooxygenase from *Acinetobacter calcoaceticus* (AcCHMO), led to rather low activities in *Syn*6803 (Böhmer et al., 2017). This is unexpected as 1) sufficient NADPH supply can be assumed under light conditions, with NADPH as the main product of the photosynthetic light reaction and 2) high-level NADPH supply was shown recently for an NADPH-dependent reductase in *Syn*6803 (Assil-Companioni et al., 2020).

In this study, we aimed to establish and scale efficient NADPH-dependent BVMO biocatalysis driven by light. To this end, we chose a BVMO from *Acidovorax* sp. CHX100 for heterologous expression in *Syn*6803. This NADPH-dependent BVMO has been shown to exhibit high activity in *Pseudomonas taiwanensis* VLB120 and used for efficient cascade designs (Schäfer et al., 2020; Bretschneider et al., 2021b). We systematically investigated how expression levels of the respective gene in *Syn*6803 can be enhanced and investigated the resulting BVMO performance in *Syn*6803. Furthermore, we examined limitations regarding gene expression, reaction kinetics, and host metabolism. Respective reaction engineering and scaling are shown to enable BVMO catalysis with an efficiency auguring well for future applications of light-driven redox biocatalysis.

MATERIALS AND METHODS

Strains, Chemicals, and Cultivation Methods

DNA oligonucleotides, plasmids, and bacterial strains used for cloning procedures are given in the Supporting Information (**Supplementary Table S1**). *Synechocystis* sp. PCC6803 (Stanier et al., 1971) was cultivated in 20 or 50 ml YBG11 medium (Shcolnick et al., 2007) with 50 mM 4-(2-hydroxyethyl)-1-piperazinethanesulfonic acid, pH 7.2, using 100 or 250 ml baffled shaking flasks with cotton stoppers, respectively. Cultivation conditions were 30°C, 150 rpm [2.5 cm amplitude], 50 $\mu mol_{photons}$ m^{-2} s^{-1}, ambient CO_2 [0.04%], 75% humidity, and start OD_{750} = 0.06–0.08. Plate cultivation was conducted on BG11 agar plates with 1.5–2.0% agar at 30°C and 25 $\mu mol_{photons}$ m^{-2} s^{-1}. If required, kanamycin (Km) was used at a final concentration of 50 µg ml^{-1}. Cyclohexanone, ≥ 99.5% purity, was purchased from Sigma-Aldrich (Steinheim, Germany). Cyclohexanol, ≥ 99% purity, was purchased from Merck (Darmstadt, Germany). All other chemicals were purchased from Carl Roth GmbH (Karlsruhe, Germany), Merck, or Sigma-Aldrich at the highest purity available.

Cloning and Transformation

Standard molecular biology procedures were applied as described by Sambrook and Russell (2001). For construction of pAH059, a

fragment coding for the C-terminal *Strep*-tagged *bvmo* gene (Schäfer et al., 2020) was amplified from pCom10_Capro (Karande et al., 2018) *via* Phusion PCR using the primer pair PAH096/097 and cloned *via* Gibson assembly (Gibson et al., 2009) into pEERM3_Km, linearized by *Xba*I/*Pst*I double digestion. For construction of pAH063, the expression cassette of P*rnsB_bvmo_Strep*-tag_terminator was amplified *via* Phusion PCR using the primer pair BVMO1/2 and cloned *via* Gibson assembly into pPMQAK1, linearized with *Eco*RI/*Pst*I double digestion. *Escherichia coli* DH5α (Hanahan, 1983) was transformed with Gibson products *via* electroporation and correct assembly of plasmids was confirmed *via* colony PCR of transformants and subsequent sequencing. Commercial kits from Macherey-Nagel (Düren, Germany) were used for plasmid DNA extraction and DNA purification.

For electroporation of *Syn*6803, cells were grown under standard conditions to an OD_{750} = 0.5–0.7 determined with a LibraS11 spectrophotometer (Biochrom, Cambridge, United Kingdom), harvested by centrifugation at 5,000 *g* and 4 °C, washed and 50 x concentrated in 1 mM 4-(2-hydroxyethyl)-1-piperazinethanesulfonic acid, pH 7.5 [according to (Ludwig et al., 2008)]. In total, 60 µl of cell suspension was supplied with 0.5–1 µg of plasmid DNA and electroporated (2.5 kV; 5 ms). After 24 h recovery in YBG11 under standard conditions, selection was performed at 25 $\mu mol_{photons}$ m^{-2} s^{-1} on BG11 agar plates containing Km. Transformants grown within 7–10 days were confirmed *via* colony PCR and sequencing. For chromosomal integration, complete segregation was achieved by iterative plating on selective agar plates with increasing Km concentration.

Protein Analysis

Exponentially growing *Syn*6803_Ni_cBVMO, *Syn*6803_Ni_pBVMO, and *Syn*6803_Cu_pBVMO cultures (see **Supplementary Table S1** for strain designations) were harvested by centrifugation at 5,000 *g* and 4°C 24 h after induction with defined concentrations of $NiSO_4$ and concentrated to an OD_{750} = 20 in 1 x TBS (1 mM phenyl-methyl-sulfonyl-fluoride, pH 7.5). Cells were disrupted in a Precellys® homogenizer for 3 cycles á 3 × 30″ with 30″ pause. After centrifugation at 13.300 *g* and 4°C for 15 min, the supernatant was used for protein concentration determination *via* the Bradford analysis (Bradford, 1976). Protein abundance was visualized using SDS-PAGE according to Laemmli (1970), with 3.6 and 12% acrylamide in the stacking and in the separation gels, respectively.

Whole-Cell Activity Assays and Determination of Reaction Kinetics

*Syn*6803_Cu_pBVMO, *Syn*6803_Ni_cBVMO, and 6803_Ni_pBVMO cultures (**Supplementary Table S1**) were harvested by centrifugation at 5,000 *g* and 4°C 24 h after induction with defined concentrations of $NiSO_4$ and adjusted to a defined cell concentration by re-suspending in YBG 11 containing 50 mM 4-(2-hydroxyethyl)-1-piperazinethanesulfonic acid and 10 µM $NiSO_4$, pH 7.2, if not stated otherwise. Cells were equilibrated for 10 min to assay conditions. Standard assay conditions were 30°C, 200 rpm, 150 $\mu mol_{photons}$ m^{-2} s^{-1}, ambient CO_2 (0.04%). The conversion of cyclohexanone (C-one) to ε-caprolactone (ε-Cl) was started by adding C-one to a final concentration of 5 mM and was stopped after 30 min by either quenching with 1 vol diethylether containing 0.2 mM *n*-decane as an internal standard (for GC analysis) or by adding 0.1 vol of acetonitrile (for HPLC analysis).

TABLE 1 | Conditions and data for Syn6803_Ni_pBVMO-based C-one biotransformation in a 2-L photo STR (Infors AG, Bottmingen, Switzerland).

Parameter	LL LC	HL LC	HL HC
Aeration			
Air [L min^{-1}]	2–0.2[a]	2–0.2[a]	2–0.2[a]
CO_2 [mL min^{-1}]	–	–	20
Light [$\mu mol_{photons}$ m^{-2} s^{-1}]			
For growth	100	150–200–250[b]	150–200–250[b]
For biotransformation	150	700	700
C-one feed [set to *U g_{CDW}^{-1}*]	25	15	30
Biomass conc.[c] *[g_{CDW} L^{-1}]*	0.55 ± 0.09	0.61 ± 0.04	1.02 ± 0.01
Product titer *[mM]*	11.6 ± 1.0 after 27 h	9.9 ± 1.6 after 25 h	11.5 ± 0.2 after 27 h

LL, low light; HL, high light; LC, low carbon; HC, high carbon, see text for details.
[a]For biotransformation, Air supply was reduced to 0.2 L min^{-1}.
[b]Stepwise increase of light intensity during growth.
[c]Biomass concentration at the start of the biotransformation, assessed via OD_{750}

For short-term assays (30 min), a cell concentration of 0.7–1 g_{CDW} L^{-1} was used in a total volume of 1 ml in 10 ml Pyrex tubes. For the investigation of whole-cell kinetics, the cell concentration was reduced to 0.25–0.5 g_{CDW} L^{-1} and the reaction time to 5 min to record initial activities.

Kinetic parameters (V_{max}, K_S and K_i) were obtained by fitting according to Michaelis–Menten kinetics with substrate inhibition using *OriginPro2019* following **Eq. 1**, where V is the specific activity in U g_{CDW}^{-1} and [S] is the substrate concentration.

$$V = \frac{V_{max} * [S]}{K_S + [S]\left(1 + \frac{[S]}{K_i}\right)} \left[\mathrm{U\ g_{CDW}}^{-1}\right] \quad (1)$$

For competitive and non-competitive inhibitors, K_s and V_{max} in **Eq. 1** were replaced by K_s' according to **Eq. 2** or V_{max}' according to **Eq. 3**, respectively, where [I] and $K_{i,I}$ are the concentration and the inhibition constant of the respective inhibitor.

$$K_S^{'} = K_S * \left(1 + \frac{[I]}{K_{i,I}}\right) [\mu M], \quad (2)$$

$$V_{max}^{'} = \frac{V_{max}}{\left(1 + \frac{[I]}{K_{i,I}}\right)} \left[\mathrm{U\ g_{CDW}}^{-1}\right] \quad (3)$$

Production Process in a 2-L Stirred Tank Photo-Bioreactor

Whole-cell biotransformations were conducted in a stirred tank photo-bioreactor Labfors 5 Lux (Infors AG, Bottmingen, Switzerland) with 2 L culture volume. Cells were grown for 3–4 days at 30°C, 2 L min^{-1} aeration with (high carbon, HC,

additional 20 ml min^{-1} CO_2) or without (low carbon, LC, no additional CO_2), 300 rpm stirrer speed, and specific light intensities (for details, see **Table 1**). Induction with 10 µM $NiSO_4$ was performed 24 h prior to biotransformation start. During biotransformation, aeration was reduced to 0.2 L min^{-1} and light intensity was set to low light (LL, 150 $\mu mol_{photons}$ m^{-2} s^{-1}) or high light (HL, 700 $\mu mol_{photons}$ m^{-2} s^{-1}). After preconditioning for 30 min, biotransformation was initiated by starting a continuous feed of 0.25 M C-one in the YBG11 medium. Samples were taken at regular time intervals and quenched immediately by adding either 1 vol diethylether or 0.1 vol acetonitrile.

Analytics

The cell concentration was assessed by determining OD_{750} in a LibraS11 spectrophotometer (Biochrom, Cambridge, United Kingdom). The previously determined correlation factor of 0.225 g_{CDW} L^{-1} per OD_{750} unit was used to calculate cell dry weight (CDW) concentrations (Hoschek et al., 2017). Chl_a concentration was determined as described by Grund et al. (2019). Concentrations of cyclohexanol (C-ol), C-one, and ε-Cl were determined by gas chromatography (GC) as described before (Schäfer et al., 2020). See **Supplementary Figure S1** for exemplary calibration curves.

Concentrations of 6-hydroxyhexanoic acid (6-HA) were determined by HPLC on a Dionex Ultimate 3,000 system equipped with an Acclaim® OA column (both Thermo Fisher Scientific, Waltham, MA). The sample was acidified with 1 M HCl to pH 3.0. The mobile phase A consisted of 100 mM sodium sulfate, adjusted with methanesulfonic acid to pH 3. Acetonitrile (>99.95% purity, ProtoChem) was used as mobile phase B. Sample volumes of 10–20 µL were injected, while the flow and the column temperature were kept constant at 0.4 ml min^{-1} and 60°C, respectively. The flow profile was as follows: 5% B for 2 min, 5–30% B in 6 min, 30–80% B in 1 min, 80% B for 1 min, 80–5% B in 2 min, and 5% B for 5.5 min. Detection was accomplished *via* a UV detector at 210 nm.

Kinetic Bioprocess Modeling

For kinetic bioprocess modeling, the Berkeley Madonna software (version 8.3.18) was used. The biotransformation converting cyclohexanone (C-one) to ε-caprolactone (ε-Cl) as a product and cylohexanol (C-ol) as a by-product was described in a kinetic model. The concentration courses for substrate (S′, C-one), product (p', ε-Cl), and by-product (B′, C-ol) were calculated using **Eqs 4–6**:

$$S' = F - kB - kP\ [\mathrm{mM\ min^{-1}}], \tag{4}$$

$$B' = kB\ [\mathrm{mM\ min^{-1}}], \tag{5}$$

and

$$P' = kP\ [\mathrm{mM\ min^{-1}}], \tag{6}$$

where the C-one feed rate F in mM min^{-1}, the reaction rate of the keto reduction kB (C-ol formation), and of ε-Cl formation kP, described in **Eqs 7**, **8**. The reaction rates kB and kP were calculated based on determined kinetic parameters (K_s and V_{max} for keto reduction and K_s, V_{max}, and $K_{i,C\text{-}one}$ for ε-Cl formation); kP was extended by the competitive inhibition by C-ol and the non-competitive inhibition by ε-Cl as follows:

$$kP = \frac{V_{max} * [S]}{K_S\left(1 + \frac{[B]}{K_{i,C-ol}}\right) + [S]\left(1 + \frac{[S]}{K_{i,C-one}}\right)} * \frac{1}{\left(1 + \frac{[P]}{K_{i,\varepsilon-Cl}}\right)} * X\ \left[\mathrm{mM\ min^{-1}}\right] \tag{7}$$

and

$$kB = \frac{Vmax * [S]}{K_i + [S]} * X\ \left[\mathrm{mM\ min^{-1}}\right], \tag{8}$$

where the biomass concentration X is in g_{CDW} L^{-1} and the inhibition constants $K_{i,C\text{-}ol}$, $K_{i,C\text{-}one}$, and $K_{i,\varepsilon\text{-}Cl}$ for C-ol (B), C-one (S), and ε-Cl (p), respectively. See section 4.4 for the exact values chosen for the kinetic parameters.

S, P, and B were initially set to 0, and the parameters X (biomass concentration in g_{CDW} L^{-1}) and F (C-one feed rate in mM min^{-1}) were fed into the model according to the respective experiment. The kinetic process model can be found in the supplemental material.

RESULTS

Plasmid-Based Ni^{2+}-Induced Gene Expression Leads to High Levels of Active BVMO

In order to systematically analyze different expression strategies in *Syn*6803, three different strains were constructed: *Syn*6803_Cu_pBVMO for plasmid-based BVMO gene expression under control of the Cu^{2+}-inducible P*petE* promoter and *Syn*6803_Ni_pBVMO and *Syn*6803_Ni_cBVMO for plasmid- and genome-based BVMO gene expression, respectively, under control of the Ni^{2+}-inducible P*nrsB* promoter. All designed strains were compared in the detail regarding protein level and specific C-one to ε-CL conversion activity in short-term assays. Activities of the Ni^{2+}-inducible strains *Syn*6803_Ni_pBVMO and *Syn*6803_Ni_cBVMO were found to increase with increasing Ni^{2+} concentration yielding maximum specific activities of 52.2 ± 0.3 (10 µM Ni^{2+}) and 23.8 ± 4.0 U g_{CDW}^{-1} (15 µM Ni^{2+}), respectively (**Figure 1A**). The keto reduction of C-one to cyclohexanol (C-ol) was found to occur at a low rate of 0.5 ± 0.2 U g_{CDW}^{-1} (for details, see *Inhibitory Effects of Substrate and By-Product Necessitate Precise Reaction Control* section). It is important to note that expression induced by 15 µM Ni^{2+} did not significantly affect growth of *Syn*6803_Ni_pBVMO, whereas this Ni^{2+} concentration slightly affected growth independently of BVMO gene expression (**Supplementary Figure S2**). Cu^{2+}-induced *Syn*6803_Cu_pBVMO yielded a maximal specific activity of 29.7 ± 0.7 U g_{CDW}^{-1} (with 0.5 µM Cu^{2+}, **Figure 1B**). Ni^{2+}-inducible systems resulted in tightly regulated expression, whereas the Cu^{2+}-inducible system showed slight leakiness and poor titratability by the inducer concentration. Due to these reasons and the lower activity obtained upon plasmid-based expression, we focused on the Ni^{2+}-inducible system and

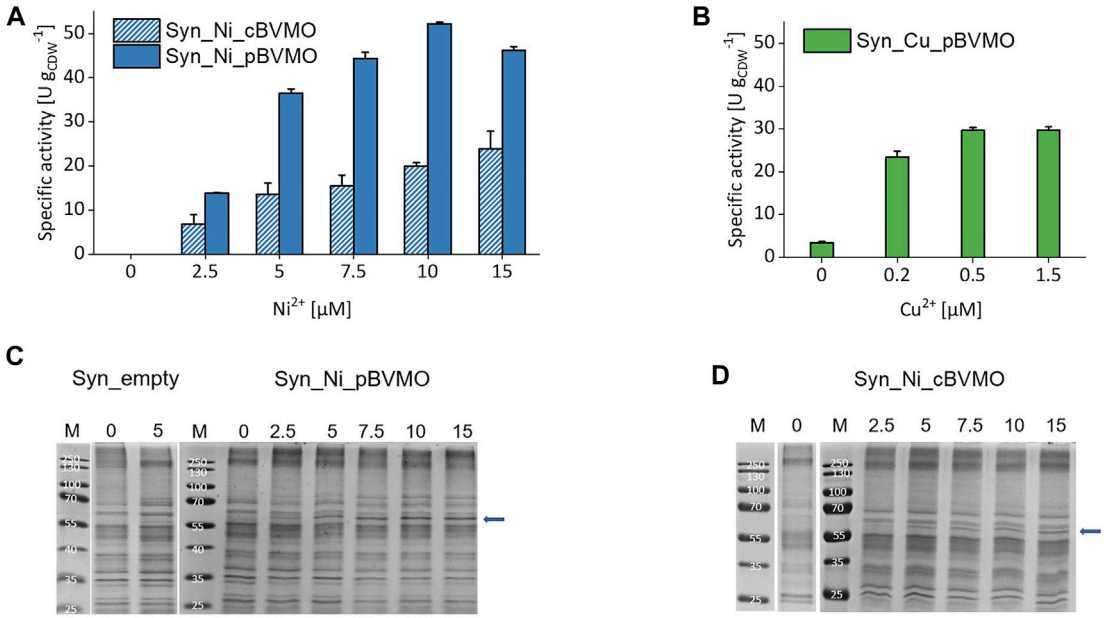

FIGURE 1 | Systematic analysis of Ni^{2+}- and Cu^{2+}-dependent specific BVMO activities **(A, B)** and expression levels **(C, D)** in modified *Syn*6803 strains. BVMO activities of **(A)** *Syn*6803_Ni_pBVMO and *Syn*6803_Ni_cBVMO and **(B)** *Syn*6803_Cu_pBVMO determined in short-term assays are given in dependence of the inducer concentration. Depicted are means from ≥2 independent measurements. N.d. not detected; 1 U = 1 µmol product formed per min. **(C,D)** SDS-PAGE gels of protein extracts upon Ni^{2+}-induced plasmid- and genome-based BVMO gene expression, respectively. Panel C also shows results for extracts of an empty vector control. Numbers above lanes indicate the Ni^{2+}-concentrations applied in µM. Arrows indicate BVMO bands (57.8 kDa); M, marker (PageRuler™).

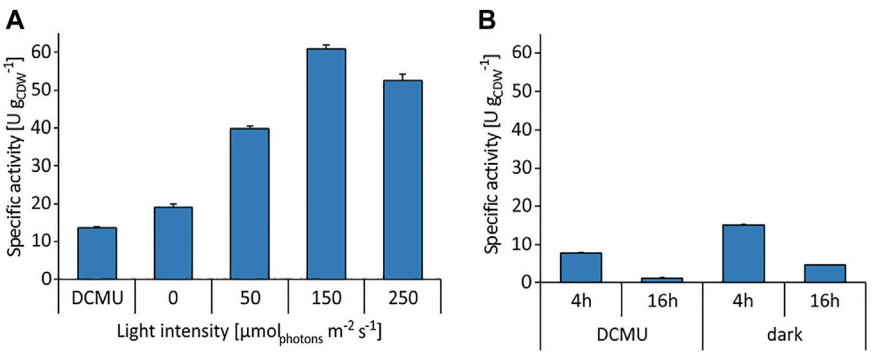

FIGURE 2 | Specific BVMO activities of *Syn*6803_Ni_pBVMO **(A)** at different light intensities and **(B)** after extended pre-incubation in absence of photosynthetic water splitting. **(A)** Cells were grown under standard conditions and equilibrated at the given light intensities for 1 h before and during the assay. DCMU: Cells were treated with PS II inhibitor DCMU (20 µM final concentration) 1 h before and during the assay and irradiated with 150 $µmol_{photons}$ m^{-2} s^{-1}. Specific activities were measured in short-term assays applying a cell concentration of 0.7–1.0 g_{CDW} L^{-1}. **(B)** Cells were grown under standard conditions and then equilibrated with DCMU (at 150 $µmol_{photons}$ m^{-2} s^{-1}) or in the dark for the given incubation times followed by an activity assay under the same conditions. Depicted are means and standard deviation of ≥3 independent experiments.

investigated plasmid- and genome-based expression in more detail. SDS-PAGE analyses of protein extracts of *Syn*6803_Ni_pBVMO and *Syn*6803_Ni_cBVMO showed a distinct band at ~60 kDa, coinciding with the BVMO size (57.8 kDa) (**Figures 1C,D**). This band intensified with increasing Ni^{2+}-concentration and was absent in un-induced cells and cells carrying an empty vector. Densitometric analysis indicated that BVMO accounted for 1.1 ± 0.2% of total soluble protein (TSP) in *Syn*6803_Ni_pBVMO induced with 10 µM Ni^{2+}, a remarkably high value for heterologous expression in *Syn*6803. Assuming a total protein content of 0.32–0.57 g g_{CDW}^{-1} (Zavrel et al., 2017), the measured specific activity of 52.2 ± 0.3 U g_{CDW}^{-1} translates into an *in vivo* activity of 7–18 U mg_{BVMO}^{-1} or a k_{cat} of 6.9–17.6 s^{-1} as a rough estimation.

In summary, we were able to construct a highly active BVMO-containing *Syn*6803 strain. Our data show that the P*nrsB*-based expression system proved to be a useful tool allowing tight,

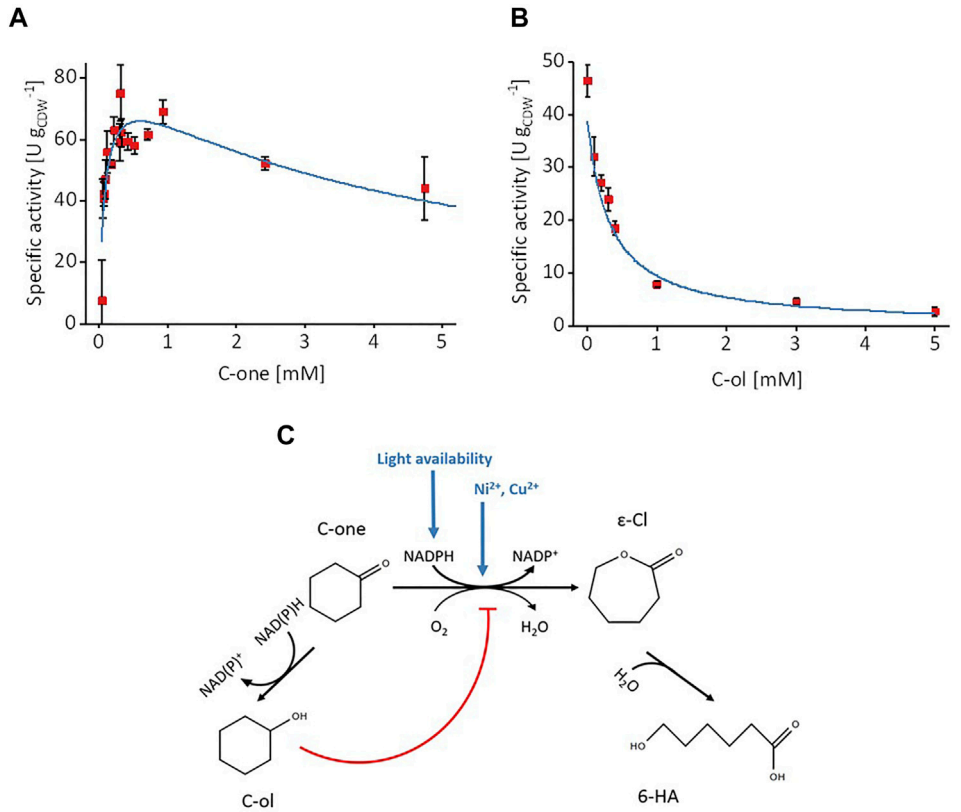

FIGURE 3 | Kinetic characterization of C-one oxidation by *Syn*6803_Ni_pBVMO. **(A)** Kinetics for C-one oxidation. Kinetic experiments were performed with 1 ml induced cells (0.25–0.5 g_{CDW} L^{-1}) in 10 ml Pyrex tubes. BVMO reactions were started by adding varying amounts of C-one (50 µM–5 mM) to cells equilibrated at standard assay conditions for 10 min and was stopped after 5 min. **(B)** Effect of C-ol on C-one oxidation activity. Varying amounts of C-ol (0–5 mM) were added to 1 ml induced cells (0.7–1.0 g_{CDW} L^{-1}) in 10 ml Pyrex tubes. Also here, cells were equilibrated for 10 min, and the reaction was started by substrate addition. Reactions were stopped after 30 min. Depicted are mean values and standard deviations from ≥2 independent experiments. **(C)** Reactions and parameters influencing ε-Cl formation by *Syn*6803: BVMO-catalyzed conversion C-one into ε-Cl; intrinsic alcohol dehydrogenases catalyze C-one reduction to C-ol, which inhibits C-one oxidation. ε-Cl is hydrolyzed to 6-HA by intrinsic hydrolases.

tunable, and high-level expression. *Syn*6803_Ni_pBVMO was thus chosen for further characterization of photosynthesis-driven BVMO catalysis.

The BVMO Reaction in *Synechocystis* sp. PCC6803 Is Light Dependent

The BVMO reaction depends on NADPH as electron donor and thus is expected to constitute an artificial electron sink and thus to depend on the major electron source in phototrophs—the photosynthetic water oxidation. To test if and to what extent the BVMO reaction in *Syn*6803 depends on incident light, short-term activity assays at light intensities ranging from 0 to 250 $\mu mol_{photons}$ m^{-2} s^{-1} were performed in medium deficient in organic compounds as potential electron donors. Clearly, specific activities increased with increasing light intensity with the maximal activity of 60.9 ± 1.0 U g_{CDW}^{-1} measured at 150 $\mu mol_{photons}$ m^{-2} s^{-1} (**Figure 2A**). With chlorophyll a content of 11.8 ± 0.8 mg_{Chla} g_{CDW}^{-1}, this activity translates into 5.2 ± 0.8 U mg_{Chla}^{-1}. Higher light intensities (such as 250 $\mu mol_{photons}$ m^{-2} s^{-1}) led to a slight activity decrease, most likely due to photoinhibitory effects. When blocking electron transfer from PS II to the PQ pool by means of the respective inhibitor 3-(3,4-dichlorphenyl)-1,1-dimethylurea (DCMU) or upon incubation in the dark, residual activities of 13.6 ± 0.3 or 19.0 ± 0.8 U g_{CDW}^{-1} were observed, respectively. These typical background/dark activities are most likely fueled by reducing equivalents derived from storage compounds. We could show that extended periods (up to 16 h) of incubation in the dark or with DCMU, which involves the consumption of storage compounds and thus a reduction of their availability, decreases the activities to 4.7 ± 0.1 and 1.3 ± 0.2 U g_{CDW}^{-1}, respectively (**Figure 2B**). These results clearly indicate a close coupling of the BVMO reaction to the photosynthetic electron transport chain.

Inhibitory Effects of Substrate and By-Product Necessitate Precise Reaction Control

To specify the optimal substrate concentration, the reaction kinetics were analyzed for *Syn*6803_Ni_pBVMO by varying the C-one concentration between 50 µM and 3 mM in 5 min assays. The cells showed Michaelis–Menten-type kinetics with

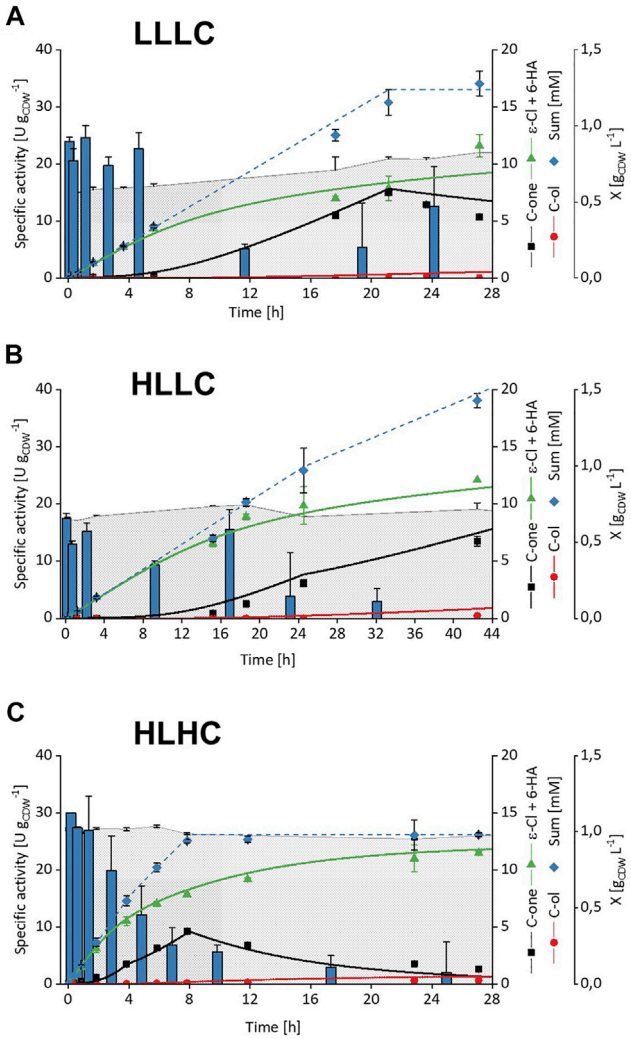

FIGURE 4 | Photosynthesis-driven C-one oxidation in a 2-L stirred tank photo-bioreactor under different light and CO2 regimes. *Syn*6803_Ni_pBVMO was grown for 3–4 days and induced with 10 μM $NiSO_4$. Biotransformations were started 24 h after induction by feeding C-one in a substrate-limited regime, for detailed parameters see **Table 1**. **(A)** Low light/low carbon (LLLC): C-one was fed at a rate matching a specific activity of 25 U g_{CDW}^{-1} for 21.5 h with an initial biomass concentration of 0.55 ± 0.09 g_{CDW} L^{-1}. **(B)** High light/low carbon (HLLC): C-one was fed at a rate matching 15 U g_{CDW}^{-1} for 24.5 h and then at a rate matching 10 U g_{CDW}^{-1}; the initial biomass concentration was 0.61 ± 0.04 g_{CDW} L^{-1}. **(C)** High light/high carbon (HLHC): C-one was fed at a rate matching 30 U g_{CDW}^{-1} for 4 h, which then was decreased by 30% until 8 h; the initial biomass concentration was of 1.02 ± 0.01 g_{CDW} L^{-1}. Experimental data are given as blue bars: specific activity in U [= μmol (ε-Cl + 6-HA) min^{-1}] g_{CDW}^{-1}; black squares: C-one in mM; green triangles: total product in mM; red circles: C-ol in mM; and blue circles: sum of all analytes in mM. Depicted are mean values and standard deviations from ≥2 technical replicates. Dashed line (blue): Total C-one fed in mM. Straight lines depict simulated courses of C-one (black), ε-Cl (green), and C-ol (red) concentrations obtained *via* Berkeley Madonna software using a model based on determined and fitted kinetic parameters (see text for details).

slight substrate inhibition (**Figure 3A**). Fitting according to Michaelis–Menten kinetics with substrate inhibition gave a reasonable fit and the following kinetic parameters: K_S = 79 ± 23 μM, V_{max} = 83.7 ± 8.0 U g_{CDW}^{-1}, and K_i = 4.4 ± 1.5 mM. This indicates that the C-one concentration is a critical reaction parameter requiring careful control.

C-one oxidation applying whole cells of both heterotrophic (Schäfer et al., 2020) and phototrophic hosts (Böhmer et al., 2017) has been reported to compete with keto reduction catalyzed by host-intrinsic enzymes, giving rise to C-ol (**Figure 3C**). This also was true for *Syn*6803_Ni_pBVMO, which was used for kinetic experiments investigating C-ol formation. Fitting according to Michaelis–Menten kinetics yielded a high K_S of 7.4 ± 0.6 mM and a comparably low V_{max} of 2.75 ± 0.15 U g_{CDW}^{-1} (**Supplementary Figure S3**). Additionally, 6-hydroxyhexanoic acid (6-HA) was detected as by-product, which can be ascribed to abiotic hydrolysis of ε-CL (**Supplementary Figure S4**). Potential inhibition by these by-products also was tested in activity assays. Whereas 6-HA did not significantly affect C-one oxidation (**Supplementary Figure S6**), C-ol was found to be a strong inhibitor with a K_i of 0.03 mM, determined *via* kinetic fittings as described in *Whole-cell activity assays and determination of reaction kinetics* section (**Figure 3B**), corresponding to a $K_{i,C\text{-}ol}/K_{s,C\text{-}one}$ ratio of 0.38. **Figure 3C** depicts a reaction scheme based on the findings described in this paragraph. Since intrinsic alcohol dehydrogenase activity can barely be avoided without drastically interfering with host metabolism, high BVMO levels can be considered pivotal to promote ε-CL formation. In this way, low yields due to by-product formation and—even more relevant—inhibition by C-ol can largely be avoided.

Gram Scale ε-Caprolactone Production in a 2-L Photo-Bioreactor

To test the long-term stability of C-one oxidation by *Syn*6803_Ni_pBVMO, we recorded the biotransformation time course in shaking flasks initially containing 5 mM C-one and fed by pulsing the same amount after 1 and 3 h. The 15 mM C-one supplied were completely converted to 14.2 ± 1.5 mM products (ε-Cl and 6-HA, **Supplementary Figure S5**). Thereby, the initial specific activity of 33 U g_{CDW}^{-1} determined for the first hour was found to decrease continuously over time. This decrease can be attributed to C-ol accumulation, reaching a final titer of 0.51 ± 0.07 mM, and intermittently high C-one concentrations leading to enforced substrate inhibition.

In order to test the feasibility of *Syn*6803_Ni_pBVMO to produce ε-Cl in the gram scale, this strain was applied in a 2-L stirred-tank photo-bioreactor (photo-STR) providing an efficient O_2 and CO_2 mass transfer and a controlled environment. The latter included the application of a limiting continuous substrate feed to minimize both substrate and by-product inhibition. To establish different source/sink conditions, light intensity (low light, LL: 150 $\mu mol_{photons}$ m^{-2} s^{-1} or high light, HL: 700 $\mu mol_{photons}$ m^{-2} s^{-1}) and CO_2 supply *via* aeration (low CO_2, LC: ambient CO_2 or high CO_2, HC, 1 and 10% CO_2 during growth and biotransformation, respectively) were varied to establish the three source/sink regimes LLLC, HLLC, and HLHC (for details, see **Table 1**).

After a growth phase of 3–4 days, including induction by adding 10 μM $NiSO_4$ 24 h before biotransformation start, C-one feeding was initiated at a fixed rate matching a specifically chosen activity. The first reactor was run with 0.55 ± 0.09 g_{CDW} L^{-1} under LLLC and a feed rate set to 25 U $g_{CDW}{}^{-1}$. A final product titer (sum of ε-Cl and 6-HA) of 11.6 ± 1.0 mM was reached after 28 h (see **Figure 4A**). However, 5.4 ± 0.1 mM C-one remained unconverted, as the specific activity strongly decreased within the first hours. A second reactor was set up for HLLC conditions to rule out light limitation as a reason for the decreasing activity. To avoid substrate accumulation, the initial substrate feed rate was adjusted to match an activity of 15 U $g_{CDW}{}^{-1}$ using 0.61 ± 0.04 g_{CDW} L^{-1}. This lead to a prolonged product formation phase, yielding however a slightly lower final product titer of 9.8 ± 1.6 mM after 25 h (**Figure 4B**). To test, if product formation benefits from higher biomass concentrations, the third photo-STR was conducted using HLHC conditions. These conditions allowed for a 70% higher initial biomass concentration (1.02 ± 0.01 g_{CDW} L^{-1}, see **Table 1**). To increase the C-one conversion rate, substrate supply was set to match 30 U $g_{CDW}{}^{-1}$. Comparable to the previous reactor runs, this preset activity of 30 U $g_{CDW}{}^{-1}$ only was met initially and was decreasing in time, resulting in C-one accumulation, requiring adjustment of the C-one feed rate (decrease to 70% after 4 h and stop of C-one feed after 8 h, **Figure 4C**). The final product titer was 11.5 ± 0.2 mM after 27 h, corresponding to a volumetric productivity of 48.6 ± 0.8 mg L^{-1} h^{-1} and a product yield of 0.88 ($mol_{ε\text{-}Cl+6\text{-}HA}$ $mol_{C\text{-}one}{}^{-1}$). Thus, all experiments led to similar product titers (9.8–11.6 mM corresponding to 1.12–1.32 g L^{-1}).

Irrespective of the applied source/sink conditions, the specific activity decreased in all setups at substrate (C-one) and by-product (C-ol) levels not expected to lead to significant inhibition (**Figures 4A–C**). The independency of initial specific activities on the applied biomass concentration (varied between 0.55 and 1.02 g_{CDW} L^{-1}) indicates that light availability did not limit the specific activity (**Table 1** and **Figures 4A–C**). This was further confirmed by light intensity variation (250 $μmol_{photons}$ m^{-2} s^{-1} *vs.* 700 μ $μmol_{photons}$ m^{-2} s^{-1}) under otherwise identical conditions as in the HLHC experiment (**Figure 4C**). This low-light high-carbon (LLHC) experiment resulted in a similar initial volumetric productivity as in the HLHC experiment corroborating that light did not limit the biocatalytic activity (**Supplementary Table S2**). These results indicate that neither inhibition by C-one or C-ol nor photosynthesis limited the biocatalytic activity. Instead, product inhibition may have prevented a more effective and stable conversion. Indeed, ε-Cl was found to compromise BVMO activity in short term assays (**Supplementary Figure S6**). As no product inhibition has been observed on the enzyme level (Schäfer et al., 2020), ε-Cl rather inhibits on a physiological level, which can best be described as a non-competitive type of inhibition. With the respective fit (**Eqs 1**, **3**), the inhibitory studies yielded a $K_{i,ε\text{-}Cl}$ of 0.83 mM.

These findings prompted us to describe the biotransformations by means of a kinetic bioprocess model using Berkeley Madonna software. The model was parametrized using the kinetic data reported in the *Potentials and Limitations of Photosynthesis-Driven Redox Biocatalysis* section, which were derived from fitting according to Michaelis–Menten kinetics with substrate inhibition (**Eq. 1**). Taking into account that this approach neglects by-product and product inhibition, which occur, but were not considered for the determination of V_{max} and $K_{i,C\text{-}one}$, these parameters were set to the upper boundaries of the fittings, namely, 91 U $g_{CDW}{}^{-1}$ and 5.9 mM. The inhibition by ε-Cl observed under assay conditions (**Supplementary Figure S6**, $K_{i,ε\text{-}Cl}$ = 0.83 mM) appeared to be less pronounced in bioreactor experiments. Thus, $K_{i,ε\text{-}Cl}$ was fitted to bioreactor data resulting in a value of 2.0 mM. This allowed to simulate concentration courses for substrate (C-one), product (ε-Cl + 6-HA), and by-product (C-ol) (depicted as lines in **Figures 4A–C**) with striking accuracy. This high simulation accuracy obtained with a mere kinetic model, not considering possible influences of light intensity and CO_2 supply variation in the experiments, indicates that C-one conversion was kinetically controlled under the conditions applied, including a physiological effect of ε-Cl, and was not influenced by the tested variation in source/sink regime.

Furthermore, the process model was used to identify optimal process parameters to handle the complex reaction kinetics, namely, the feed regime and the biocatalyst concentration. For this purpose, only reaction kinetics were considered, and avoidance of a possible light limitation was assumed. To explore the sensitivity regarding the biocatalyst concentration, values of 0.5, 1, 2, and 5 g_{CDW} L^{-1} were chosen, being aware that high cell concentrations such as 5 g_{CDW} L^{-1} would involve light limitation issues in the experimental setup (as further discussed in the *Potentials and Limitations of Photosynthesis-Driven Redox Biocatalysis* section). Thereby, the feed regime applied in the HLHC experiment (**Figure 4C**) was scaled to different biocatalyst concentrations (**Figure 5A**). The highest biomass concentration tested (5 g_{CDW} L^{-1}) indeed yielded the highest product titer (17.0 mM) but accumulated C-one (36.9 mM) and C-ol (11.4 mM) in high amounts. To avoid extreme substrate and by-product accumulation and thereby optimize product titer and yield, a more conservative C-one feed was targeted. To this end, an ideal C-one conversion rate was calculated by considering product inhibition only and neglecting substrate and by-product inhibition, reflecting the upper limit of C-one supply which can be handled by the catalyst. This continuously decreasing rate was translated into a feed rate followed by simulation using the kinetic model, again testing different biocatalyst concentrations. Irrespective of the initial feed rate (30, 20, or 10 U g_{CDW} L^{-1}, **Figures 5B–D**), the overall picture remained the same: Higher biocatalyst concentrations (2 and 5 g_{CDW} L^{-1}) heavily accumulated C-one and—to a minor extent—C-ol, limiting product formation. Although lower biocatalyst concentrations (0.75 and 1 g_{CDW} L^{-1}) suffered less C-one accumulation and consequential C-ol formation, the final product titer did not exceed 10.7 mM. To conclude, the "optimized" C-one feed regime led to only a moderate increase in final product titer compared to the HLHC experiment (15.5 *vs.* 11.5 mM), but only with 5 times higher biocatalyst concentration and thus on the cost of low biocatalyst-based yield (0.4 *vs.* 1.3 g $_{ε\text{-}Cl+6\text{-}HA}$ $g_{CDW}{}^{-1}$) and product yield (0.15 *vs.* 0.88 $mol_{ε\text{-}Cl+6\text{-}HA}$ $mol_{C\text{-}one}{}^{-1}$). With the

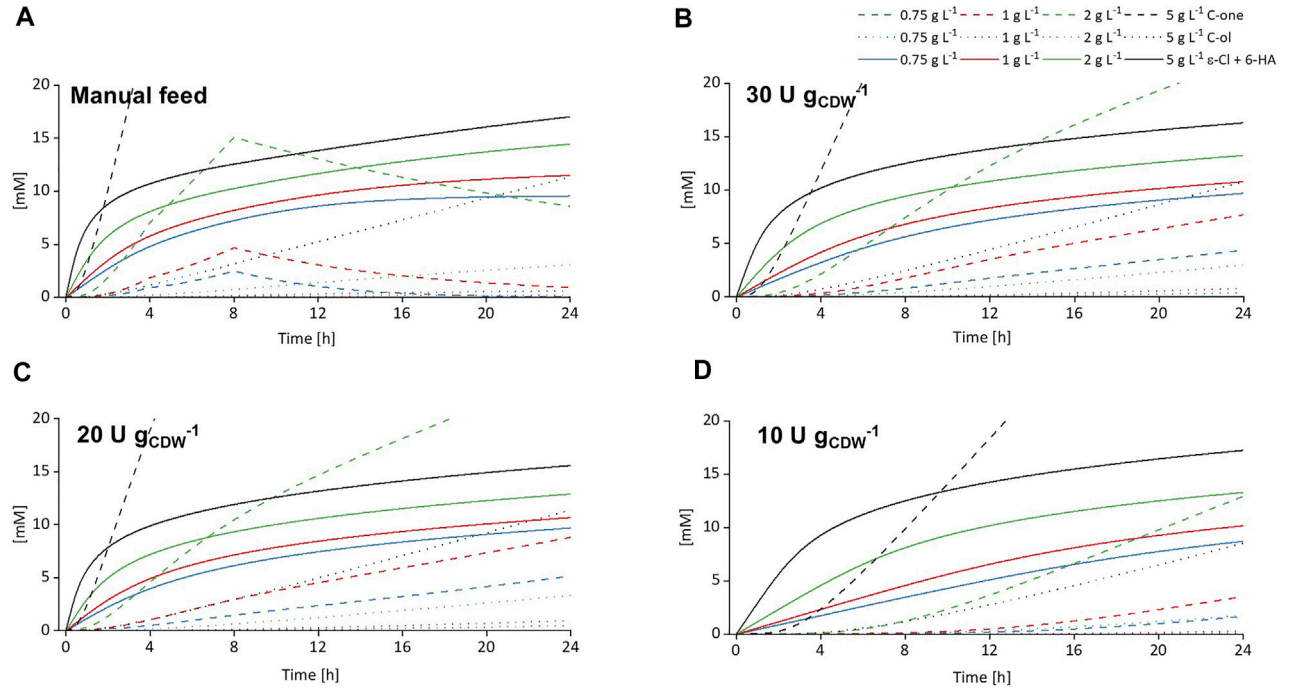

FIGURE 5 | Simulation and sensitivity analysis of the BVMO process applying the kinetic process model with **(A)** manual and **(B, C)**, and **(D)** optimized feeding regimes, with 30 U $gCDW^{-1}$, 20 U $gCDW^{-1}$, and 10 U $gCDW^{-1}$, respectively. **(A)** The feed regime applied for the HLHC reactor (see **Figure 4**) was translated to 0.75, 1.0, 2.0, and 5.0 g_{CDW} L^{-1} for a sensitivity analysis regarding the biocatalyst concentration (B/C/D). An ideal C-one conversion rate based on initial rates of 30/20/10 U $g_{CDW}{}^{-1}$, respectively, was calculated by considering product inhibition only and neglecting substrate and by-product inhibition. This reflects the upper limit of C-one supply which can be handled by the catalyst. The conversion rate was translated into a feed rate, followed by simulations using the kinetic process model with cell concentrations of 0.75, 1.0, 2.0, and 5.0 g_{CDW} L^{-1} (blue, red, green, and black lines), to test the system's sensitivity towards the biocatalyst concentration. Depicted are concentrations of C-one, C-ol, and ε-Cl in dashed, dotted, and straight lines, respectively.

same biocatalyst concentration as in the HLHC experiment, the achieved product titer was even lower (10.7 *vs.* 11.5 mM), which emphasizes the strong impact of the by-product C-ol demanding a more aggressive feed rate decrease. Overall, the reaction system remains intricate, as product titer and yield are not only restricted by product inhibition but also by the *difficile* interplay between competitive by-product inhibition and the formation of this by-product: A high substrate concentration can counteract competitive inhibition but simultaneously increases inhibitor formation. Importantly, assuming the absence of light limitation for higher cell densities did not enable significantly higher product titers than experimentally obtained, reemphasizing that kinetic restrictions are the primary factors limiting the performance of the investigated reaction system.

DISCUSSION

Photosynthesis is the central biochemical transformation process converting light energy into chemical energy and therefore a highly attractive module for environmentally friendly industrial processes. It can be exploited for biotechnology by making use of photosynthetically active microorganisms such as cyanobacteria (Barber, 2009); (Angermayr et al., 2009). Their capability to fix CO_2 gives rise to the conversion of CO_2 into organic chemicals such as biofuels (Gao et al., 2016). *Inter alia*, the production of ethanol (Gao et al., 2012), 2,3-butanediol (Oliver et al., 2013), glycerol (Savakis et al., 2015), and 1-butanol (Atsumi et al., 2009) has been investigated, typically achieving rather low productivities, not exceeding 10 mg L^{-1} h^{-1}. These processes mainly suffer low energy efficiency as respective metabolic pathways are linked to carbon fixation and central carbon metabolism, which are evolutionary optimized for biomass formation under given conditions and not explicitly with respect to energy efficiency. One option to increase light-to-product energy efficiency is to link production processes closer to the photosynthetic electron transport chain and thus avoid downstream energy loss (Barber, 2009).

Following this idea, recent studies focused on the utilization of photosynthesis-derived electrons for redox biocatalysis. The coupling is realized either by directly linking electron consuming enzymes to PS I (Lassen et al., 2014a; Appel et al., 2020) or *via* reduced cofactors produced by the light reaction (Hoschek et al., 2019b; Assil-Companioni et al., 2020), for example, NADPH as in the presented study. This approach is particularly elegant for oxygenation reactions as not only electron supply but also O_2 supply—often a limiting factor in aerobic large-scale bioprocesses—is realized *in situ via* photosynthetic water oxidation (Hoschek et al., 2018). In this study, the use of a 2-L stirred tank photo-bioreactor setup enabled light-driven ε-Cl

formation in the gram scale within 1 day exemplifying the potential of this approach.

Enhanced Gene Expression Makes *Synechocystis* sp. PCC6803 an Attractive Biocatalyst

The development and application of photosynthetically active microorganisms as microbial hosts is still restricted by the limited availability of molecular biology tools and the comparably poor knowledge on cell metabolism and physiology. Here, we investigated different expression systems regarding expression levels and specific activities of BVMO from *Acidovorax* sp. CHX100 in *Syn*6803. The Ni^{2+}-inducible P*nrsB* promoter system was found to enable high BVMO expression levels and be superior to the Cu^{2+}-inducible P*petE* promoter system in terms of inducibility and expression level, in accordance with previous studies (Englund et al., 2016; Liang et al., 2018). It is important to note that the expression level achieved with a promoter depends on the genetic context (Englund et al., 2016). The expression levels of up to 1.1 ± 0.2% of TSP reached in this study are to our best knowledge unprecedented with the P*nrsB* system in *Syn*6803. Numerous studies have characterized different controllable promoter systems in *Syn*6803: non-native ones such as the LacI-repressible P*trc*1O system (Huang et al., 2010), the TetR-regulated L03 promoter (Huang and Lindblad, 2013), and other P*lac* variants (Thiel et al., 2018) as well as native ones like Cu^{2+}-inducible P*petE* (Briggs et al., 1990) and Ni^{2+}-inducible P*nrsB* promoters (Englund et al., 2016). However, most studies focused on the optimization of expression systems rather than on designing suitable biocatalysts and use fluorescent proteins as read-out for expression strength. Thus, not much is known about the cellular concentrations of heterologous protein. For catalytically active enzymes, such as dehydrogenases or monooxygenases (Lassen et al., 2014a), constitutive systems, such as the discovered "super strong" promoter P*cpc*560 (Zhou et al., 2014) or the light-inducible promoter P*psbA*, have been applied (Wang et al., 2018). They yield high expression levels up to 15% (Zhou et al., 2014) and 12.6% of TSP (Wang et al., 2018). However, for oxygenase biocatalysis, well-steerable promoter systems are more desirable to control metabolic burden such as ROS formation. They yield lower but still remarkable expression levels of 0.4% (Sebesta and Peebles, 2020) and 1.1% of TSP (Savakis et al., 2015), of which the latter was met by *Syn*6803_Ni_pBVMO generated in this study.

With P*nrsB*, plasmid-based expression yielded a 2.6 times higher BVMO level and activity than chromosome-based expression (**Figure 1**). This difference may be due to a higher copy number of the plasmid than the chromosome (Huang et al., 2010). It however has been reported that the copy number of pPMQAK1 is comparable to that of the chromosome (Jin et al., 2018). Such contradiction has been explained by the observation that both plasmid and chromosome copy numbers vary strongly in *Syn*6803 (Heidorn et al., 2011). This makes chromosomal integration the more laborious method due to the necessity for segregation, whereas the plasmid-based approach can suffer instability and the necessity for constant antibiotic selection (Kadisch et al., 2017).

The strong correlation of specific BVMO activity and the expression level (**Figure 1**) suggests that the achieved BVMO level still limits the biocatalyst activity. Future advances regarding molecular biology tools for cyanobacteria can be expected to enable even higher biocatalyst activities. Promising candidate expression systems include the recently characterized rhamnose-inducible promoter P*rhaBAD* (Kelly et al., 2018) or the vannilate-inducible promoter *P*vanCC (Behle et al., 2020).

Photosynthesis-Driven BVMO Catalysis Is Hampered by Reactant Inhibition Rather Than Host Metabolism

BVMO containing *Syn*6803 was found to feature a 3.7 times lower apparent uptake constant K_S for C-one (80 ± 23 μM) than *Pseudomonas taiwanensis* VLB 120 containing the same enzyme (316 ± 21 μM) (Bretschneider et al., 2021a). This indicates a rather efficient substrate mass transfer into the cell. Furthermore, we observed moderate substrate inhibition, an often encountered effect with BVMOs (Scherkus et al., 2017; Fürst et al., 2019; Schmidt and Bornscheuer, 2020). The host metabolic background interferes with the biotransformation in terms of C-one reduction to C-ol as reported before (Böhmer et al., 2017), but with a rather low V_{max} (2.75 ± 0.15 mM) and a rather high K_S (7.4 ± 0.6 mM). More important was the inhibition of BVMO activity by C-ol already at low concentrations (K_i = 0.03 mM). This is in agreement with published data on heterotrophs containing the same enzyme (Schäfer et al., 2020), indicating an inhibitory effect on the enzyme level. To reduce formation of the (inhibiting) by-product, the introduction of an enzyme for re-conversion of C-ol to C-one could be an interesting solution (Bayer et al., 2017). Deletion of intrinsic alcohol dehydrogenases constitute another option but may harm cell viability and thus be tedious. Taken together, these data show that controlling substrate concentration is key for efficient photosynthesis-driven BVMO catalysis.

The optimized strain *Syn*6803_Ni_pBVMO reached a maximal specific activity of 60.9 ± 1.0 U g_{CDW}^{-1}. This is around 4 to 5 times lower than published for the heterotrophic host *Pseudomonas taiwanensis* VLB120 (Schäfer et al., 2020), which showed significantly higher BVMO expression levels (Bretschneider et al., 2021a) and features a highly active energy and redox metabolism based on organic acids and sugars (Volmer et al., 2014). It is however noteworthy that the BVMO exhibited a much higher *in vivo* activity in *Syn*6803 than in *P. taiwanensis*, that is, a 4.6 to 11 times higher k_{cat} (6.9–17.6 s^{-1} *vs.* 1.5 s^{-1} (Bretschneider et al., 2021a)). It should be noted that BVMO catalysis in *Syn*6803 appeared not to be limited by the metabolic capacity to supply reduction equivalents as the photoproduction of NADPH in *Syn*6803 is in the range of 9–18 U mg Chl_a (Kauny and Setif, 2014), which translates to 106–212 U g_{CDW}^{-1}. Presumably, this limitation was decisive for BVMO catalysis in *P. taiwanensis*. The activities achieved already indicate the great potential of *Syn*6803 as host for energy-dependent biotransfomations. Future research efforts to fill

knowledge gaps regarding expression systems, other molecular biology tools, and cofactor regeneration can be expected to further improve photosynthesis-driven biotransformation efficiency (Hitchcock et al., 2020).

Despite keeping by-product and substrate strictly below inhibiting values, the biocatalyst performance was found to be compromised in the long term. Neither increased light nor CO_2 supply had a positive effect (**Figure 4B**). Instead, the product ε-Cl itself was found to affect biocatalyst performance (**Supplementary Figure S6**). Such product inhibition also was the decisive limitation in simulations based on kinetic data, which overall fit well the bioreactor data. Interestingly, product inhibition was not detected with heterotrophic hosts (Schäfer et al., 2020) and seems to be *Syn*6803 specific. Effects of ε-Cl on *Syn*6803 physiology may involve inhibition of metabolism leading to NADPH limitation as discussed below. To address product inhibition, *in situ* product removal technologies can be applied (Dafoe and Daugulis, 2014). Whereas two liquid-phase approaches are compromised by the intermediary polarity of the product, solid-phase extraction may be a promising but costly solution. Alternatively, BVMO catalysis can be amended by a lipase (Scherkus et al., 2017) or lactonase (Schäfer et al., 2020) reaction to obtain 6-HA which is less problematic in terms of inhibition but still feasible as a polymer precursor.

Potentials and Limitations of Photosynthesis-Driven Redox Biocatalysis

The biocatalyst-based yield ($g_{Product}\ g_{CDW}^{-1}$) has been proposed as an important measure for catalyst performance (Fürst et al., 2019). *Syn*6803_Ni_pBVMO reached a yield of 1.3 and 1.6 $g_{Product}\ g_{CDW}^{-1}$ in a 2-L photo-bioreactor and in shaking flasks, respectively. A sensitivity analysis based on the kinetic model affirmed a yield of 1.5 $g_{Product}\ g_{CDW}^{-1}$ to be realistic for the used bioreactor setup. This is on the same level as an industry-relevant BVMO-based process with *Escherichia coli* featuring a yield of 1.6 $g_{Product}\ g_{CDW}^{-1}$ for a however more complex product (Woo et al., 2018). However, phototrophic processes are not on the same readiness level as heterotrophic biocatalytic processes: It should be noted that the abovementioned metric neglects the immense differences in cell densities applied. The mentioned *E. coli*–based process uses around 25-times higher biomass concentrations than those applied in this study and thus features a higher volumetric productivity. On the other hand, *Syn*6803-based biocatalyst production, regeneration, and operation are based on CO_2 as carbon and water as electron source, making the addition of an organic carbon and energy source such as glucose dispensable. Future improvements of reactor design and cultivation strategies such as the use of capillary biofilm reactor concepts (Karande et al., 2014; Hoschek et al., 2019a) or immobilized cells (Vajravel et al., 2020) and internal illumination (Hobisch et al., 2021) are expected to push the boundaries of phototrophic cultivation/process operation. Already noteworthy are the initial and 24 h-average productivity (187 ± 1 mg $L^{-1}\ h^{-1}$ and 59 ± 1 mg $L^{-1}\ h^{-1}$, respectively), ranging among the highest productivities for biotransformations using cyanobacteria. Additionally, the product yield of 0.88 ($mol_{\varepsilon\text{-Cl+6-HA}}\ mol_{C\text{-one}}^{-1}$) prefigures the high potential of phototrophic hosts for biocatalysis.

The comparably high *in vivo* BVMO activity obtained in this study indicates that—sufficient light supply provided—NADPH can efficiently be withdrawn from phototrophic metabolism to fuel productive reactions. As confirmed by process simulation merely based on whole-cell reaction kinetics, the photosynthesis-based NADPH supply capacity did not limit the biotransformation, with efficient illumination as a prerequisite. The product itself might interfere with NADPH supply at higher concentrations by affecting membrane integrity (Sikkema et al., 1995) and thus photosynthetic electron transfer. In contrast, electron consuming redox biotransformations catalyzed by the ene-reductase Yqjm were found to be limited by NADPH availability at activities above 150 U g_{CDW}^{-1} (Assil-Companioni et al., 2020). By inactivating the proteins Flv1/Flv3, an approach known to reduce electron loss to unproductive O_2 reductions (Thiel et al., 2019), *Syn*6803 reached specific activities up to 170 U g_{CDW}^{-1}. It has to be investigated though, if this elevated electron supply can be sustained in the long term.

As oxygenases are prone to uncouple, that is, reduce O_2 without concomitant substrate oxidation, ROS formation represents another electron sink increasing the electron demand. Furthermore, ROS formation possibly affects photosynthetic metabolism (Nishiyama et al., 2005). Cyanobacteria have evolved different mechanisms to cope with and detoxify ROS (Latifi et al., 2009), which however involves additional electron/energy investment further increasing the electron demand.

Today, the disposability of electrons from water oxidation, for example, by water electrolysis, is a field of particular interest, especially for H_2 production. In this context, envisaged light-to-H_2 solutions using cyanobacterial photosynthesis as a transformation module are highly attractive (Appel et al., 2020). Success towards this goal relies, beside O_2 tolerance of biocatalysts and high cell-density cultivation concepts, on the electron supply capacity of photoautotrophic microbes. It is still unclear, if a high electron demand for technically feasible H_2 production can be met by cells still able to sustain themselves. Interestingly, additional electron sinks were shown to increase photosynthetic efficiency and thereby electron fluxes through the photosynthetic apparatus (Zhou et al., 2016; Grund et al., 2019). This observation reinforces the sink-limitation hypothesis, which states that photosynthesis is rather limited by the availability of electron sinks than by electron (energy) sources (Berepiki et al., 2016). This gives the possibility to tap unused electron supply potential for electron consuming reactions. Limits of and factors influencing electron supply *via* the photosynthetic light reaction for biotechnological application remain to be investigated. Reductases, such as Yqjm (Assil-Companioni et al., 2020), and oxygenases, such as the cycloalkane hydroxylating cytochrome P450 monoxygenase (Hoschek et al., 2019b) and the BVMO investigated in this study, have now been established as prominent electron sinks in cyanobacteria and constitute excellent blueprints to decipher the potential of the

photosynthetic light reaction as electron source for biotechnological application.

DATA AVAILABILITY STATEMENT

The original contributions presented in the study are included in the article/**Supplementary Materials**; further inquiries can be directed to the corresponding authors.

AUTHOR CONTRIBUTIONS

AT, AS, BB, and JT were involved in the conception and design of the study. AT, MU, and FN performed experimental work and collected data. AT, BB, and JT did data curation and interpretation. AT wrote the original draft of the manuscript. BB and JT contributed in terms of article structuring and editing. All authors were involved in editing and approved the submitted version.

FUNDING

AT is funded by the German National Academic Foundation.

ACKNOWLEDGMENTS

We acknowledge the use of the facilities of the Centre for Biocatalysis (MiKat) at the Helmholtz Centre for Environmental Research, which is supported by European Regional Development Funds (EFRE, Europe funds Saxony) and the Helmholtz Association.

SUPPLEMENTARY MATERIAL

The Supplementary Material for this article can be found online at: https://www.frontiersin.org/articles/10.3389/fctls.2021.780474/full#supplementary-material

REFERENCES

Angermayr, S. A., Hellingwerf, K. J., Lindblad, P., and Teixeira de Mattos, M. J. (2009). Energy Biotechnology with Cyanobacteria. *Curr. Opin. Biotechnol.* 20 (3), 257–263. doi:10.1016/j.copbio.2009.05.011

Appel, J., Hueren, V., Boehm, M., and Gutekunst, K. (2020). Cyanobacterial *In Vivo* Solar Hydrogen Production Using a Photosystem I-Hydrogenase (PsaD-HoxYH) Fusion Complex. *Nat. Energ.* 5, 458–467. doi:10.1038/s41560-020-0609-6

Assil-Companioni, L., Büchsenschütz, H. C., Solymosi, D., Dyczmons-Nowaczyk, N. G., Bauer, K. K. F., Wallner, S., et al. (2020). Engineering of NADPH Supply Boosts Photosynthesis-Driven Biotransformations. *ACS Catal.* 10 (20), 11864–11877. doi:10.1021/acscatal.0c02601

Atsumi, S., Higashide, W., and Liao, J. C. (2009). Direct Photosynthetic Recycling of Carbon Dioxide to Isobutyraldehyde. *Nat. Biotechnol.* 27 (12), 1177–1180. doi:10.1038/nbt.1586

Baldwin, C. V. F., and Woodley, J. M. (2006). On Oxygen Limitation in a Whole Cell Biocatalytic Baeyer-Villiger Oxidation Process. *Biotechnol. Bioeng.* 95 (3), 362–369. doi:10.1002/bit.20869

Barber, J. (2009). Photosynthetic Energy Conversion: Natural and Artificial. *Chem. Soc. Rev.* 38 (1), 185–196. doi:10.1039/b802262n

Bayer, T., Milker, S., Wiesinger, T., Winkler, M., Mihovilovic, M. D., and Rudroff, F. (2017). *In Vivo* Synthesis of Polyhydroxylated Compounds from a "Hidden Reservoir" of Toxic Aldehyde Species. *ChemCatChem* 9 (15), 2919–2923. doi:10.1002/cctc.201700469

Behle, A., Saake, P., Germann, A. T., Dienst, D., and Axmann, I. M. (2020). Comparative Dose-Response Analysis of Inducible Promoters in Cyanobacteria. *ACS Synth. Biol.* 9, 843–855. doi:10.1021/acssynbio.9b00505

Berepiki, A., Hitchcock, A., Moore, C. M., and Bibby, T. S. (2016). Tapping the Unused Potential of Photosynthesis with a Heterologous Electron Sink. *ACS Synth. Biol.* 5 (12), 1369–1375. doi:10.1021/acssynbio.6b00100

Berla, B. M., Saha, R., Immethun, C. M., Maranas, C. D., Moon, T. S., and Pakrasi, H. B. (2013). Synthetic Biology of Cyanobacteria: Unique Challenges and Opportunities. *Front. Microbiol.* 4, 246. doi:10.3389/fmicb.2013.00246

Böhmer, S., Köninger, K., Gómez-Baraibar, Á., Bojarra, S., Mügge, C., Schmidt, S., et al. (2017). Enzymatic Oxyfunctionalization Driven by Photosynthetic Water-Splitting in the Cyanobacterium Synechocystis Sp. PCC 6803. *Catalysts* 7 (8), 240. doi:10.3390/catal7080240

Bornscheuer, U. T., Huisman, G. W., Kazlauskas, R. J., Lutz, S., Moore, J. C., and Robins, K. (2012). Engineering the Third Wave of Biocatalysis. *Nature* 485 (7397), 185–194. doi:10.1038/nature11117

Bradford, M. M. (1976). A Rapid and Sensitive Method for the Quantitation of Microgram Quantities of Protein Utilizing the Principle of Protein-Dye Binding. *Anal. Biochem.* 72, 248–254. doi:10.1016/0003-2697(76)90527-3

Bretschneider, L., Heuschkel, I., Ahmed, A., Bühler, K., Karande, R., and Bühler, B. (2021a). Characterization of Different Biocatalyst Formats for BVMO-catalyzed Cyclohexanone Oxidation. *Biotechnol. Bioeng.* 118, 2719–2733. doi:10.1002/bit.27791

Bretschneider, L., Wegner, M., Bühler, K., Bühler, B., and Karande, R. (2021b). One-pot Synthesis of 6-aminohexanoic Acid from Cyclohexane Using Mixed-species Cultures. *Microb. Biotechnol.* 14 (3), 1011–1025. doi:10.1111/1751-7915.13744

Briggs, L. M., Pecoraro, V. L., and McIntosh, L. (1990). Copper-induced Expression, Cloning, and Regulatory Studies of the Plastocyanin Gene from the Cyanobacterium Synechocystis Sp. PCC 6803. *Plant Mol. Biol.* 15 (4), 633–642. doi:10.1007/BF00017837

Burk, M. J., and Van Dien, S. (2016). Biotechnology for Chemical Production: Challenges and Opportunities. *Trends Biotechnol.* 34 (3), 187–190. doi:10.1016/j.tibtech.2015.10.007

Camsund, D., and Lindblad, P. (2014). Engineered Transcriptional Systems for Cyanobacterial Biotechnology. *Front. Bioeng. Biotechnol.* 2, 40. doi:10.3389/fbioe.2014.00040

Dafoe, J. T., and Daugulis, A. J. (2014). *In Situ* product Removal in Fermentation Systems: Improved Process Performance and Rational Extractant Selection. *Biotechnol. Lett.* 36 (3), 443–460. doi:10.1007/s10529-013-1380-6

Englund, E., Liang, F., and Lindberg, P. (2016). Evaluation of Promoters and Ribosome Binding Sites for Biotechnological Applications in the Unicellular Cyanobacterium Synechocystis Sp. PCC 6803. *Sci. Rep.* 6, 36640. doi:10.1038/srep36640

Fürst, M. J. L. J., Gran-Scheuch, A., Aalbers, F. S., and Fraaje, M. W. (2019). Baeyer-Villiger Monooxygenases: Tunable Oxidative Biocatalysts. *ACS Catal.* 9, 11207–11241. doi:10.10.21/acscatal.9b03396

Gale, G. A. R., Schiavon Osorio, A. A., Mills, L. A., Wang, B., Lea-Smith, D. J., and McCormick, A. J. (2019). Emerging Species and Genome Editing Tools: Future Prospects in Cyanobacterial Synthetic Biology. *Microorganisms* 7 (10), 409. doi:10.3390/microorganisms7100409

Gao, X., Sun, T., Pei, G., Chen, L., and Zhang, W. (2016). Cyanobacterial Chassis Engineering for Enhancing Production of Biofuels and Chemicals. *Appl. Microbiol. Biotechnol.* 100 (8), 3401–3413. doi:10.1007/s00253-016-7374-2

Gao, Z., Zhao, H., Li, Z., Tan, X., and Lu, X. (2012). Photosynthetic Production of Ethanol from Carbon Dioxide in Genetically Engineered Cyanobacteria. *Energy Environ. Sci.* 5 (12), 9857–9865. doi:10.1039/C2EE22675H

Gibson, D. G., Young, L., Chuang, R.-Y., Venter, J. C., Hutchison, C. A., 3rd, and Smith, H. O. (2009). Enzymatic Assembly of DNA Molecules up to Several Hundred Kilobases. *Nat. Methods* 6 (5), 343–345. doi:10.1038/nmeth.1318

Gordon, G. C., and Pfleger, B. F. (2018). Regulatory Tools for Controlling Gene Expression in Cyanobacteria. *Adv. Exp. Med. Biol.* 1080, 281–315. doi:10.1007/978-981-13-0854-3_12

Grund, M., Jakob, T., Wilhelm, C., Bühler, B., and Schmid, A. (2019). Electron Balancing under Different Sink Conditions Reveals Positive Effects on Photon Efficiency and Metabolic Activity of Synechocystis Sp. PCC 6803. *Biotechnol. Biofuels* 12, 43. doi:10.1186/s13068-019-1378-y

Hanahan, D. (1983). Studies on Transformation of *Escherichia coli* with Plasmids. *J. Mol. Biol.* 166 (4), 557–580. doi:10.1016/s0022-2836(83)80284-8

Heidorn, T., Camsund, D., Huang, H.-H., Lindberg, P., Oliveira, P., Stensjö, K., et al. (2011). Synthetic Biology in Cyanobacteria. *Methods Enzymol.* 497, 539–579. doi:10.1016/B978-0-12-385075-1.00024-X

Hitchcock, A., Hunter, C. N., and Canniffe, D. P. (2020). Progress and Challenges in Engineering Cyanobacteria as Chassis for Light-driven Biotechnology. *Microb. Biotechnol.* 13 (2), 363–367. doi:10.1111/1751-7915.13526

Hobisch, M., Spasic, J., Malihan-Yap, L., Barone, G. D., Castiglione, K., Tamagnini, P., et al. (2021). Internal Illumination to Overcome the Cell Density Limitation in the Scale-up of Whole-Cell Photobiocatalysis. *ChemSusChem* 14 (15), 3219–3225. doi:10.1002/cssc.202100832

Hoschek, A., Bühler, B., and Schmid, A. (2017). Overcoming the Gas-Liquid Mass Transfer of Oxygen by Coupling Photosynthetic Water Oxidation with Biocatalytic Oxyfunctionalization. *Angew. Chem. Int. Ed.* 56 (47), 15146–15149. doi:10.1002/anie.201706886

Hoschek, A., Heuschkel, I., Schmid, A., Bühler, B., Karande, R., and Bühler, K. (2019a). Mixed-species Biofilms for High-Cell-Density Application of Synechocystis Sp. PCC 6803 in Capillary Reactors for Continuous Cyclohexane Oxidation to Cyclohexanol. *Bioresour. Technol.* 282, 171–178. doi:10.1016/j.biortech.2019.02.093

Hoschek, A., Schmid, A., and Bühler, B. (2018). *In Situ* O2Generation for Biocatalytic Oxyfunctionalization Reactions. *ChemCatChem* 10 (23), 5366–5371. doi:10.1002/cctc.201801262

Hoschek, A., Toepel, J., Hochkeppel, A., Karande, R., Bühler, B., and Schmid, A. (2019b). Light-Dependent and Aeration-Independent Gram-Scale Hydroxylation of Cyclohexane to Cyclohexanol by CYP450 Harboring Synechocystis Sp. PCC 6803. *Biotechnol. J.* 14 (8), 1800724. doi:10.1002/biot.201800724

Huang, H.-H., Camsund, D., Lindblad, P., and Heidorn, T. (2010). Design and Characterization of Molecular Tools for a Synthetic Biology Approach towards Developing Cyanobacterial Biotechnology. *Nucleic Acids Res.* 38 (8), 2577–2593. doi:10.1093/nar/gkq164

Huang, H.-H., and Lindblad, P. (2013). Wide-dynamic-range Promoters Engineered for Cyanobacteria. *J. Biol. Eng.* 7 (1), 10. doi:10.1186/1754-1611-7-10

Imamura, S., and Asayama, M. (2009). Sigma Factors for Cyanobacterial Transcription. *Gene Regul Syst. Bio* 3, 65–87. doi:10.4137/grsb.s2090

Immethun, C. M., and Moon, T. S. (2018). "Synthetic Gene Regulation in Cyanobacteria," in *Synthetic Biology of Cyanobacteria*. Editors W. Zhang and X. Song ((Singapore: Springer), 317–355. doi:10.1007/978-981-13-0854-3_13

Jin, H., Wang, Y., Idoine, A., and Bhaya, D. (2018). Construction of a Shuttle Vector Using an Endogenous Plasmid from the Cyanobacterium Synechocystis Sp. PCC6803. *Front. Microbiol.* 9, 1662. doi:10.3389/fmicb.2018.01662

Jodlbauer, J., Rohr, T., Spadiut, O., Mihovilovic, M. D., and Rudroff, F. (2021). Biocatalysis in Green and Blue: Cyanobacteria. *Trends Biotechnol.* 39, 875–889. doi:10.1016/j.tibtech.2020.12.009

Johnson, C. H., and Golden, S. S. (1999). Circadian Programs in Cyanobacteria: Adaptiveness and Mechanism. *Annu. Rev. Microbiol.* 53, 389–409. doi:10.1146/annurev.micro.53.1.389

Kadisch, M., Willrodt, C., Hillen, M., Bühler, B., and Schmid, A. (2017). Maximizing the Stability of Metabolic Engineering-Derived Whole-Cell Biocatalysts. *Biotechnol. J.* 12 (8), 1600170. doi:10.1002/biot.201600170

Karande, R., Halan, B., Schmid, A., and Buehler, K. (2014). Segmented Flow Is Controlling Growth of Catalytic Biofilms in Continuous Multiphase Microreactors. *Biotechnol. Bioeng.* 111 (9), 1831–1840. doi:10.1002/bit.25256

Karande, R., Salamanca, D., Schmid, A., and Buehler, K. (2018). Biocatalytic Conversion of Cycloalkanes to Lactones Using an *In-Vivo* cascade in Pseudomonas Taiwanensis VLB120. *Biotechnol. Bioeng.* 115 (2), 312–320. doi:10.1002/bit.26469

Kauny, J., and Sétif, P. (2014). NADPH Fluorescence in the Cyanobacterium Synechocystis Sp. PCC 6803: a Versatile Probe for *In Vivo* Measurements of Rates, Yields and Pools. *Biochim. Biophys. Acta (Bba) - Bioenerg.* 1837 (6), 792–801. doi:10.1016/j.bbabio.2014.01.009

Kelly, C. L., Taylor, G. M., Hitchcock, A., Torres-Méndez, A., and Heap, J. T. (2018). A Rhamnose-Inducible System for Precise and Temporal Control of Gene Expression in Cyanobacteria. *ACS Synth. Biol.* 7 (4), 1056–1066. doi:10.1021/acssynbio.7b00435

Laemmli, U. K. (1970). Cleavage of Structural Proteins during the Assembly of the Head of Bacteriophage T4. *Nature* 227 (5259), 680–685. doi:10.1038/227680a0

Lassen, L. M., Nielsen, A. Z., Olsen, C. E., Bialek, W., Jensen, K., Møller, B. L., et al. (2014a). Anchoring a Plant Cytochrome P450 via PsaM to the Thylakoids in Synechococcus Sp. PCC 7002: Evidence for Light-Driven Biosynthesis. *PLoS One* 9 (7), e102184. doi:10.1371/journal.pone.0102184

Lassen, L. M., Nielsen, A. Z., Ziersen, B., Gnanasekaran, T., Møller, B. L., and Jensen, P. E. (2014b). Redirecting Photosynthetic Electron Flow into Light-Driven Synthesis of Alternative Products Including High-Value Bioactive Natural Compounds. *ACS Synth. Biol.* 3 (1), 1–12. doi:10.1021/sb400136f

Latifi, A., Ruiz, M., and Zhang, C.-C. (2009). Oxidative Stress in Cyanobacteria. *FEMS Microbiol. Rev.* 33 (2), 258–278. doi:10.1111/j.1574-6976.2008.00134.x

Law, H. E. M., Baldwin, C. V. F., Chen, B. H., and Woodley, J. M. (2006). Process Limitations in a Whole-Cell Catalysed Oxidation: Sensitivity Analysis. *Chem. Eng. Sci.* 61, 6646–6652. doi:10.1016/j.ces.2006.06.007

Liang, F., Englund, E., Lindberg, P., and Lindblad, P. (2018). Engineered Cyanobacteria with Enhanced Growth Show Increased Ethanol Production and Higher Biofuel to Biomass Ratio. *Metab. Eng.* 46, 51–59. doi:10.1016/j.ymben.2018.02.006

Ludwig, A., Heimbucher, T., Gregor, W., Czerny, T., and Schmetterer, G. (2008). Transformation and Gene Replacement in the Facultatively Chemoheterotrophic, Unicellular Cyanobacterium Synechocystis Sp. PCC6714 by Electroporation. *Appl. Microbiol. Biotechnol.* 78 (4), 729–735. doi:10.1007/s00253-008-1356-y

Nishiyama, Y., Allakhverdiev, S. I., and Murata, N. (2005). Inhibition of the Repair of Photosystem II by Oxidative Stress in Cyanobacteria. *Photosynth Res.* 84 (1-3), 1–7. doi:10.1007/s11120-004-6434-0

Oliver, J. W. K., Machado, I. M. P., Yoneda, H., and Atsumi, S. (2013). Cyanobacterial Conversion of Carbon Dioxide to 2,3-butanediol. *Proc. Natl. Acad. Sci. USA* 110 (4), 1249–1254. doi:10.1073/pnas.1213024110

Sambrook, J., and Russell, D. W. (2001). *Molecular Cloning : A Laboratory Manual. Cold Spring Harbor*. N.Y.: Cold Spring Harbor Laboratory Press.

Savakis, P., Tan, X., Du, W., Branco dos Santos, F., Lu, X., and Hellingwerf, K. J. (2015). Photosynthetic Production of Glycerol by a Recombinant Cyanobacterium. *J. Biotechnol.* 195, 46–51. doi:10.1016/j.jbiotec.2014.12.015

Schäfer, L., Bühler, K., Karande, R., and Bühler, B. (2020). Rational Engineering of a Multi-Step Biocatalytic Cascade for the Conversion of Cyclohexane to Polycaprolactone Monomers in Pseudomonas Taiwanensis. *Biotechnol. J.* 15, 2000091. doi:10.1002/biot.202000091

Scherkus, C., Schmidt, S., Bornscheuer, U. T., Gröger, H., Kara, S., and Liese, A. (2017). Kinetic Insights into ϵ-caprolactone Synthesis: Improvement of an Enzymatic cascade Reaction. *Biotechnol. Bioeng.* 114 (6), 1215–1221. doi:10.1002/bit.26258

Schmid, A., Dordick, J. S., Hauer, B., Kiener, A., Wubbolts, M., and Witholt, B. (2001). Industrial Biocatalysis Today and Tomorrow. *Nature* 409 (6817), 258–268. doi:10.1038/35051736

Schmidt, S., and Bornscheuer, U. T. (2020). Baeyer-Villiger Monooxygenases: From Protein Engineering to Biocatalytic Applications. *Enzymes* 47, 231–281. doi:10.1016/bs.enz.2020.05.007

Schrewe, M., Julsing, M. K., Bühler, B., and Schmid, A. (2013). Whole-cell Biocatalysis for Selective and Productive C-O Functional Group Introduction and Modification. *Chem. Soc. Rev.* 42 (15), 6346–6377. doi:10.1039/c3cs60011d

Sebesta, J., and Peebles, C. A. (2020). Improving Heterologous Protein Expression in Synechocystis Sp. PCC 6803 for Alpha-Bisabolene Production. *Metab. Eng. Commun.* 10, e00117. doi:10.1016/j.mec.2019.e00117

Shcolnick, S., Shaked, Y., and Keren, N. (2007). A Role for mrgA, a DPS Family Protein, in the Internal Transport of Fe in the Cyanobacterium Synechocystis Sp. PCC6803. *Biochim. Biophys. Acta (Bba) - Bioenerg.* 1767 (6), 814–819. doi:10.1016/j.bbabio.2006.11.015

Sikkema, J., de Bont, J. A., and Poolman, B. (1995). Mechanisms of Membrane Toxicity of Hydrocarbons. *Microbiol. Rev.* 59 (2), 201–222. doi:10.1128/mr.59.2.201-222.1995

Stanier, R. Y., Kunisawa, R., Mandel, M., and Cohen-Bazire, G. (1971). Purification and Properties of Unicellular Blue-green Algae (Order Chroococcales). *Bacteriol. Rev.* 35 (2), 171–205. doi:10.1128/br.35.2.171-205.1971

Thiel, K., Mulaku, E., Dandapani, H., Nagy, C., Aro, E.-M., and Kallio, P. (2018). Translation Efficiency of Heterologous Proteins Is Significantly Affected by the Genetic Context of RBS Sequences in Engineered Cyanobacterium Synechocystis Sp. PCC 6803. *Microb. Cell Fact* 17 (1), 34. doi:10.1186/s12934-018-0882-2

Thiel, K., Patrikainen, P., Nagy, C., Fitzpatrick, D., Pope, N., Aro, E.-M., et al. (2019). Redirecting Photosynthetic Electron Flux in the Cyanobacterium Synechocystis Sp. PCC 6803 by the Deletion of Flavodiiron Protein Flv3. *Microb. Cell Fact* 18 (1), 189. doi:10.1186/s12934-019-1238-2

Till, P., Toepel, J., Bühler, B., Mach, R. L., and Mach-Aigner, A. R. (2020). Regulatory Systems for Gene Expression Control in Cyanobacteria. *Appl. Microbiol. Biotechnol.* 104 (5), 1977–1991. doi:10.1007/s00253-019-10344-w

Vajravel, S., Sirin, S., Kosourov, S., and Allahverdiyeva, Y. (2020). Towards Sustainable Ethylene Production with Cyanobacterial Artificial Biofilms. *Green. Chem.* 22 (19), 6404–6414. doi:10.1039/D0GC01830A

Volmer, J., Neumann, C., Bühler, B., and Schmid, A. (2014). Engineering of Pseudomonas Taiwanensis VLB120 for Constitutive Solvent Tolerance and Increased Specific Styrene Epoxidation Activity. *Appl. Environ. Microbiol.* 80 (20), 6539–6548. doi:10.1128/AEM.01940-14

Wang, B., Eckert, C., Maness, P.-C., and Yu, J. (2018). A Genetic Toolbox for Modulating the Expression of Heterologous Genes in the Cyanobacterium Synechocystis Sp. PCC 6803. *ACS Synth. Biol.* 7 (1), 276–286. doi:10.1021/acssynbio.7b00297

Wlodarczyk, A., Gnanasekaran, T., Nielsen, A. Z., Zulu, N. N., Mellor, S. B., Thøfner, J. F. B., et al. (2016). Metabolic Engineering of Light-Driven Cytochrome P450 Dependent Pathways into Synechocystis Sp. PCC 6803. *Metab. Eng.* 33, 1–11. doi:10.1016/j.ymben.2015.10.009

Woo, J.-M., Jeon, E.-Y., Seo, E.-J., Seo, J.-H., Lee, D.-Y., Yeon, Y. J., et al. (2018). Improving Catalytic Activity of the Baeyer-Villiger Monooxygenase-Based *Escherichia coli* Biocatalysts for the Overproduction of (Z)-11-(heptanoyloxy)undec-9-enoic Acid from Ricinoleic Acid. *Sci. Rep.* 8 (1), 10280. doi:10.1038/s41598-018-28575-8

Zavřel, T., Očenášová, P., and Červený, J. (2017). Phenotypic Characterization of Synechocystis Sp. PCC 6803 Substrains Reveals Differences in Sensitivity to Abiotic Stress. *PLoS One* 12 (12), e0189130. doi:10.1371/journal.pone.0189130

Zhou, J., Zhang, F., Meng, H., Zhang, Y., and Li, Y. (2016). Introducing Extra NADPH Consumption Ability Significantly Increases the Photosynthetic Efficiency and Biomass Production of Cyanobacteria. *Metab. Eng.* 38, 217–227. doi:10.1016/j.ymben.2016.08.002

Zhou, J., Zhang, H., Meng, H., Zhu, Y., Bao, G., Zhang, Y., et al. (2014). Discovery of a Super-strong Promoter Enables Efficient Production of Heterologous Proteins in Cyanobacteria. *Sci. Rep.* 4, 4500. doi:10.1038/srep04500

Conflict of Interest: The authors declare that the research was conducted in the absence of any commercial or financial relationships that could be construed as a potential conflict of interest.

Publisher's Note: All claims expressed in this article are solely those of the authors and do not necessarily represent those of their affiliated organizations, or those of the publisher, the editors, and the reviewers. Any product that may be evaluated in this article, or claim that may be made by its manufacturer, is not guaranteed or endorsed by the publisher.